Climate Dynamics (2023) 60:227–238
https://doi.org/10.1007/s00382-022-06319-9

Representation of sea ice regimes in the Western Ross Sea, Antarctica, based on satellite imagery and AMPS wind data

Usama Farooq[1] · Wolfgang Rack[1] · Adrian McDonald[1,2] · Stephen Howell[3]

Received: 17 December 2020 / Accepted: 24 April 2022 / Published online: 20 May 2022

Abstract

Sea ice drift data at high spatial resolution and surface wind model output are used to explore atmosphere-sea ice interactions in the Western Ross Sea including the three main polynyas areas; McMurdo Sound polynya (MSP), Terra Nova Bay polynya (TNBP), and the Ross Sea polynya (RSP). This study quantifies the relationship between the winds and sea ice drift and observes the average and annual anomalies across the region. Sea ice drift velocities are based on high-resolution (150 m) Advanced Synthetic Aperture Radar (ASAR) images from Envisat for winters between 2002 and 2012. Sea ice motion vectors were first correlated with the corresponding Antarctic Mesoscale Prediction System (AMPS) surface wind velocities, and the sensitivity of the spatial correlations and residuals were examined. Four drift parameters were selected (mean drift, the correlation between drift and wind, drift to wind scaling factor, and the directional drift constancy) to perform an unsupervised k-means classification to automatically distinguish six zones of distinctive sea ice characteristics solely based on ice drift and wind information. Results indicate a heterogeneous pattern of sea ice movement at a rate ranging from 0.41 to 2.24% of the wind speed in different areas. We also find that the directional constancy of sea ice drift is closely related to the wind fields. Sea ice drift and wind velocities display the highest correlation in free-drift areas (R = 0.70), followed by deformational drift zones (R = 0.54), and more random drift areas (R = 0.28). The classification illustrates the significance of localized wind-driven sea ice drift in this coastal area resulting in zones of convergence, shear, and free drift. The results also indicate that the most persistent patterns of sea ice motion are near the RSP and TNBP areas, both being driven by strong localized winds. Our findings identify that large-scale sea ice motion is predominantly wind-driven over much of the study area while ocean currents play only a minor role.

Keywords Sea ice drift · Wind forcing · Envisat ASAR · AMPS · Sea ice classification · Antarctica · Western Ross Sea

1 Introduction

Sea ice drift is forced by winds and ocean currents and is a vital element in the dynamics of the polar oceans (Leppäranta, 2011). Sea ice drift can provide valuable information about the governing thermodynamic and dynamic processes forming sea ice and its role within the Antarctic climate system (Notz, 2012). Sea ice motion in the Antarctic is normally monitored either by buoy data (e.g., Doble and Wadhams, 2006; Heil and Allison, 1999) or by low spatial resolution satellite data (e.g., Kimura, 2004; Kwok et al., 2017). Buoy observations only provide sparse measurements of the sea ice drift but offer high temporal resolution information at a small number of locations. Coarse spatial resolution satellite data can provide the overall basin-wide motion pattern but are limited in providing accurate monitoring on the regional basis, and studies suggest that the error margins can be high (Farooq et al., 2020; Kwok et al., 2017).

Sea ice motion derived from satellite observations has improved our understanding of large-scale dynamics in the Antarctic (Holland and Kwok, 2012). However, sea ice dynamics, thermodynamics, and surface winds need to be correctly represented in climate models to obtain the correct

✉ Usama Farooq
usama.farooq@pg.canterbury.ac.nz

[1] Gateway Antarctica, University of Canterbury, 8140 Christchurch, New Zealand

[2] School of Physical and Chemical Sciences, University of Canterbury, 8140 Christchurch, New Zealand

[3] Climate Research Division, Environment and Climate Change Canada, Toronto, Ontario, Canada

trends of sea ice area in historical analyses (Holland and Kwok, 2012; Holmes et al., 2019). In Antarctica, the coastal polynyas also have a significant role in the formation, advection, and deformation of sea ice (Dale et al., 2017, Rack et al., 2020). These atmospherically forced polynyas also play an essential role in the formation of High Salinity Shelf Water and Antarctic Bottom Water formation (Jacobs, 2004). As a result, there is a need to accurately estimate sea ice motion and transport from the polynya areas.

The spatial pattern of sea ice motion is related to atmospheric and oceanographic forcing (Thorndike and Colony, 1982). In the Southern Ocean, sea ice is moving between 10 and 20 degrees left of the wind direction, and sea ice motion is less than 2.5% of the forcing wind speed, derived using ten years (1992–2001) of coarse resolution satellite data (150 km) (Kimura, 2004). Holland and Kwok (2012) used 100 km spatial resolution data from 1992 to 2010 and found that the sea ice concentration trends are mostly wind-driven although the relationship between wind patterns and sea ice trends need further investigations (Holland and Kwok, 2012; Roach et al., 2020). Later work detailed in Kwok et al. (2017) used 34 years of satellite data from 1982 to 2015 to show that the Antarctic sea ice motion is 1.4% of the average geostrophic wind and described 40% of sea ice drift variance. Their study also documented a high error of 3 to 4 km/day in sea ice motion estimates and the requirement of using data at high spatial and temporal resolution to better estimate sea ice drift.

In the Antarctic, the Ross Sea region is considered a complex area and includes three main polynyas: McMurdo Sound Polynya (MSP), Terra Nova Bay Polynya (TNBP), and Ross Sea Polynya (RSP) (Fig. 1). The RSP is formed to the east of Ross Island in the central and western Ross Sea; the smaller MSP is located adjacent to fast ice on the coast next to the Transantarctic Mountains. The TNPB is formed directly to the north of the Drygalski ice tongue. The Ross Sea ice extent has been increasing during the past 40 years of satellite records but the trend substantially declined from 2014 and again started to increase in 2017 (Parkinson, 2019). Numerous mechanisms have been used to explain this trend, including changes in winds, ocean stratification, and/or precipitation, and sea surface temperature (Blanchard-Wrigglesworth et al., 2021; Turner et al., 2017). Kwok (2005) investigated the Ross Sea ice motion and area flux through a 1400 km wide flux gate (Land Bay to Cape Adare; red dotted line in Fig. 1), and noting a positive trend in the ice area flux between 1992 and 2003. Hollands and Dierking (2016) utilized a multi-sensor approach to derive the sea ice drift in Terra Nova Bay and analysed the temporal changes of polynya structure, extension, and

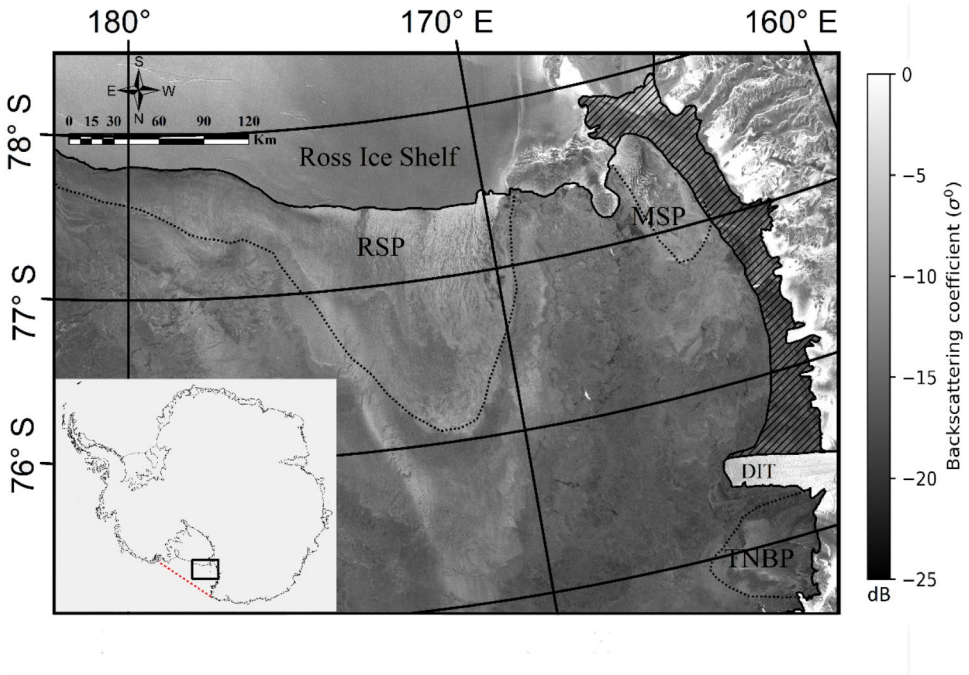

Fig. 1 Envisat SAR image (16 June 2011) in the polar-stereographic projection showing the study area of the Western Ross Sea with typical extent of three prominent polynyas (dashed lines): the Ross Sea Polynya (RSP), Terra Nova Bay Polynya (TNBP), and McMurdo Sound Polynya (MSP). The hatched area shows maximum land-fast sea ice for 2011. The Ross Ice Shelf (RIS) and Drygalski Ice Tongue (DIT) are also labelled. Over the Ross Sea, the variation in the grey scale is due to the different age and roughness of sea ice. High intensity backscatter coefficient (σ^o) in the RSP and MSP area represents high surface roughness in open water due to wind during an ongoing polynya event

area. Farooq et al. (2020) used Synthetic Aperture Radar (SAR) images to examine sea ice drift in the Western Ross Sea region and compared this with low-resolution sea ice motion products. They showed that the sea ice motion was underestimated significantly by low-resolution datasets and also highlighted the utility of high-resolution sea ice drift products to reduce the error in the sea ice drift analysis.

In this study, we add to the existing body of limited literature on sea ice motion in the South Western Ross sea ice by investigating the details of the wind forcing on the sea ice motion from 2002 to 2012. We focus on sea ice drift patterns in relation to the variable wind regimes, ocean currents, and geophysical sea ice properties and estimate the importance of the various contributing factors. This study addresses gaps in previous studies by using high spatial resolution sea ice motion vectors in the Ross Sea region during the entire Envisat operational period and examining the atmospheric and oceanographic forcing on the sea ice motion.

2 Description of sea ice dynamics and input data

2.1 Sea ice motion equation

The equation for sea ice motion or momentum balance equation can be derived using Newton's second law. The forces acting on a sea ice floe of mass M causing acceleration a are (Leppäranta, 2011);

$$Force = Ma = \tau_a + \tau_w + F_c + F_i + F_t \quad (1)$$

where, τ_a is air drag, τ_w represents water drag, F_c is Coriolis force, F_i shows internal ice force, and F_t is sea-surface tilt force. The equation treats the ice as a two-dimensional continuum instead of discrete particles. For thin and less-compact ice, the magnitude of the last three terms is commonly negligible compared to the first two terms in the above equation (Leppäranta, 2011).

Using the geostrophic wind G above the atmospheric boundary layer, Thorndike and Colony (1982) described the sea ice velocity u as a balance between the pressure gradient force and Coriolis force, which can be defined by a simple linear relationship.

$$u = \boldsymbol{A}G + \bar{c} + \epsilon \quad (2)$$

where, $\boldsymbol{A} = Ae^{-i\theta}$ is a complex coefficient with the turning angle (θ), $\bar{c}$ is the mean ocean current, and ε is a residual quantity of sea ice velocity which is neither a linear function nor a constant function of winds (Thorndike and Colony, 1982). The magnitude of A is commonly expressed as a mean scaling factor, which relates the average magnitudes of wind speed and ice drift (denoted F in this manuscript). In reality, the relationship between wind and drift can be non-linear, as the general equation above ignores time-dependent effects, internal stresses, and non-geostrophic components (Weiss, 2013), which are especially important in near coastal areas with significant ice deformation. Near the coast, we expect the residual ε to be spatially highly variable because of

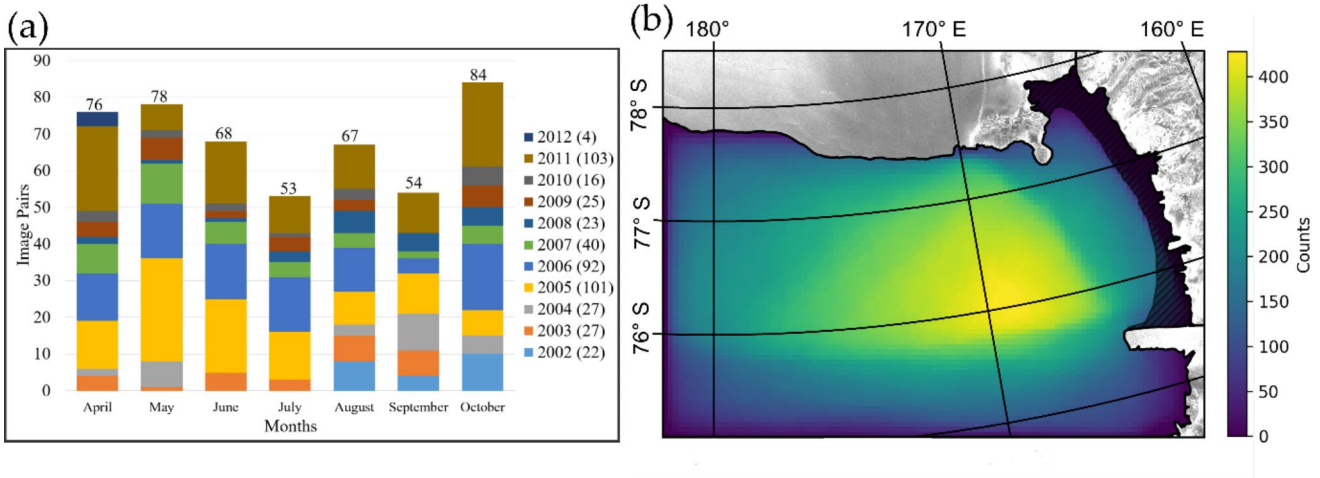

Fig. 2 (a) Bar chart showing the monthly distribution of total available one-day separated 480 sea ice velocity fields derived from Envisat satellite images from 2002–2012 during the Antarctic winter months of April – October with a complete coverage. Numbers in the parentheses showing the year-wise distribution of vector fields (b) Number of populated vectors from the 480 fields covering the study area from 2002–2012 showing that the center of the image always has maximum vectors; however, TNBP has fewer derived vectors

time-dependent ocean currents, local wind patterns, internal ice stresses by ice deformation, and observational errors (Thomas, 1999). Here we quantify on a pixel-to-pixel basis the average wind to drift relationship over ten years and use information such as the scaling factor to delineate areas of distinct sea ice evolution and deformation.

2.2 Sea ice drift data

The derivation of high spatial resolution sea ice drift vectors for our study area is described in detail in Farooq et al. (2020), and a summary is given here. Briefly, sea ice drift has been estimated using consecutive high-resolution Envisat Advanced Synthetic Aperture Radar (ASAR) images. The wide swath mode images having 150 m nominal resolution, HH polarization, and a swath width of 400 km are acquired around 18:00 UTC for the study area. The existing data from April to October have been analysed because of the nearly maximum sea ice coverage (Dale et al., 2017), from 2002 to 2012. The monthly and annual distribution of the 480 sea ice vector fields having a one-day separation is shown in Fig. 2a. The number of sea ice motion vectors calculated from the Environment and Climate Change Canada (ECCC) automatic sea ice motion tracking system (Howell et al., 2022)is shown in Fig. 2b. The root mean square error of the ECCC sea ice motion tracking algorithm is 0.43 km/day and a detailed description of the algorithm can be found in Komarov and Barber (2014). The algorithm was validated for this region with manually drawn vectors and found a high Pearson correlation coefficient of 0.98 ± 0.02 with an angle deviation of -0.79 ± 2.0 degrees (Farooq et al., 2020). The TNBP is a much more dynamic area compared to the other polynyas. The small number of vectors identified because of frequent periods of open water make it difficult to draw any conclusions in this area.

2.3 Wind data

Model outputs from the operational Antarctic Mesoscale Prediction System (AMPS) are used to examine wind speed and direction over the study area (Bromwich et al., 2005). The real-time Weather Research and Forecasting Model (WRF) forecasting system runs over five domains over Antarctica in the AMPS prediction system (Powers et al., 2012). We used archived 3-hourly, 10 m height wind data in domain 3 that covers our study area. Data for the study between April to October come in 5 km, 6.6 km, and 10 km spatial resolution for the 2009–2012, 2006–2008, and 2002–2005 periods, respectively. As the wind data are available at a 3-hourly period, eight wind fields correspond to the sea ice drift vector field calculated from 18:00 UTC to 18:00 UTC (satellite images acquired around 24 h apart).

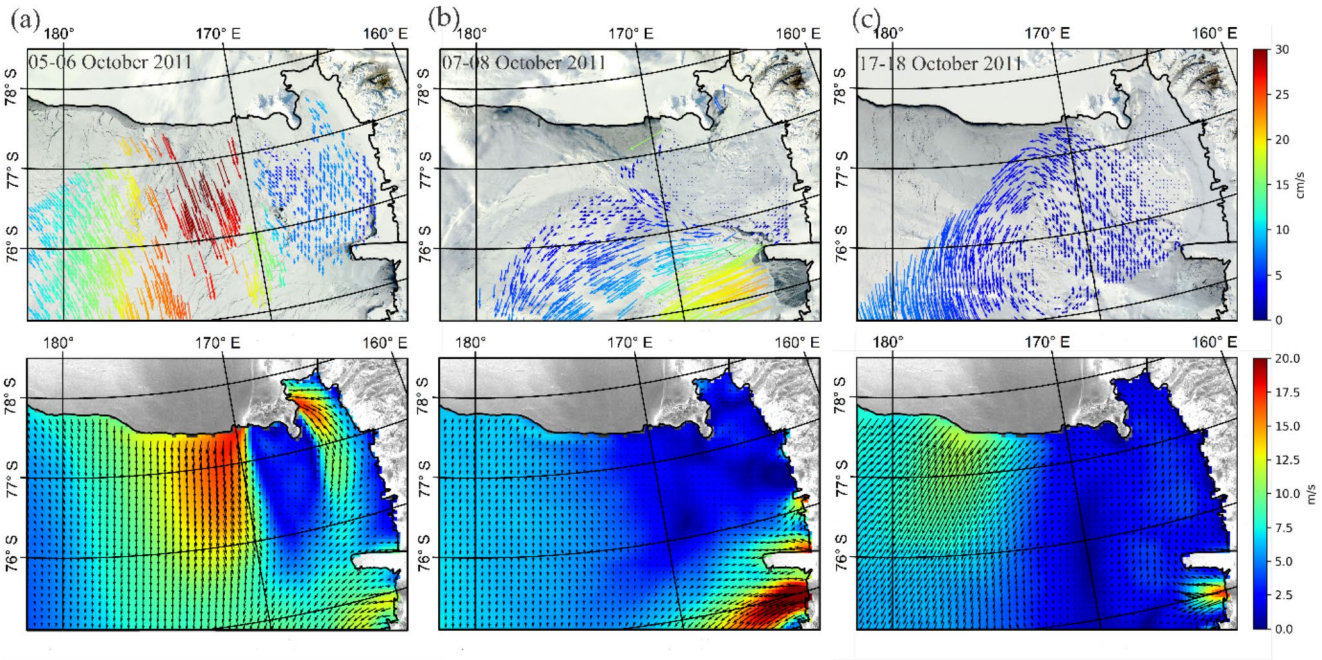

Fig. 3 Sample images showing the high visual resemblance between the sea ice drift (top row) and average prevailing wind (bottom row). Sea ice motion vectors (cm/s) are overlaid on the corresponding day MODIS image to visualize the sea ice conditions. Average wind speeds (m/s) are calculated from the eight corresponding 3-hourly wind data (a) 05–06 October 2011 (b) 07–08 October 2011 and (c) 17–18 October 2011

Therefore, eight wind fields are available for one sea ice vector field. We choose to average those eight wind fields to obtain 24 h average wind fields. For consistency, the wind data from 2002 to 2008 were scaled to 5 km by using a cubic interpolation method.

3 Data analysis and results of sea ice regimes

3.1 Fine-scale sea ice motion and wind fields

SAR derived sea ice motion fields were analysed in comparison with wind fields to perform a detailed analysis of the response of sea ice drift to atmospheric forcing. For each day, we analyzed the sea ice motion field derived from sequential SAR images with the corresponding wind field and calculated the Pearson correlation coefficient at every pixel position. Figure 3 shows samples of the sea ice motion fields and the corresponding 24-hour average wind fields for a few representative cases. One example shows the wind and drift patterns related to the Ross Ice Shelf Air Stream (RAS; Fig. 3a). RAS events are strong southerly winds from the Ross Ice Shelf (RIS) formed as a consequence of synoptic-scale cyclones aligned with the barrier presented by the Transantarctic Mountains and katabatic drainage (Parish et al. 2006); they result in the frequent opening of the Ross Sea polynya (Dale et al., 2017). Strong katabatic winds from the Transantarctic Mountains into Terra Nova Bay are responsible for the opening of the Terra Nova Bay Polynya and strong ice drift in an easterly direction (Van Woert, 1999; our Fig. 3b). The drift pattern as a result of a low-pressure system over the southwestern Ross Sea is shown in Fig. 3c. It is also observed that even the shear zones in front of the Drygalski ice tongue in Fig. 3b can be considered as wind-driven.

3.2 Average sea ice speed and wind speed

The average conditions of the study area are summarized by plotting the average sea ice motion vectors and wind field from 2002 to 2012 in Fig. 4a and b, respectively. The high frequency of open ocean and very thin ice in TNB as a consequence of polynya formation hinders the detection of sea ice drift vectors. This is a direct consequence of low sea ice concentrations as a result of very strong katabatic winds (Aulicino et al., 2019). The average wind speed over the study period is highest in TNBP (~ 16 m/s) followed by RSP

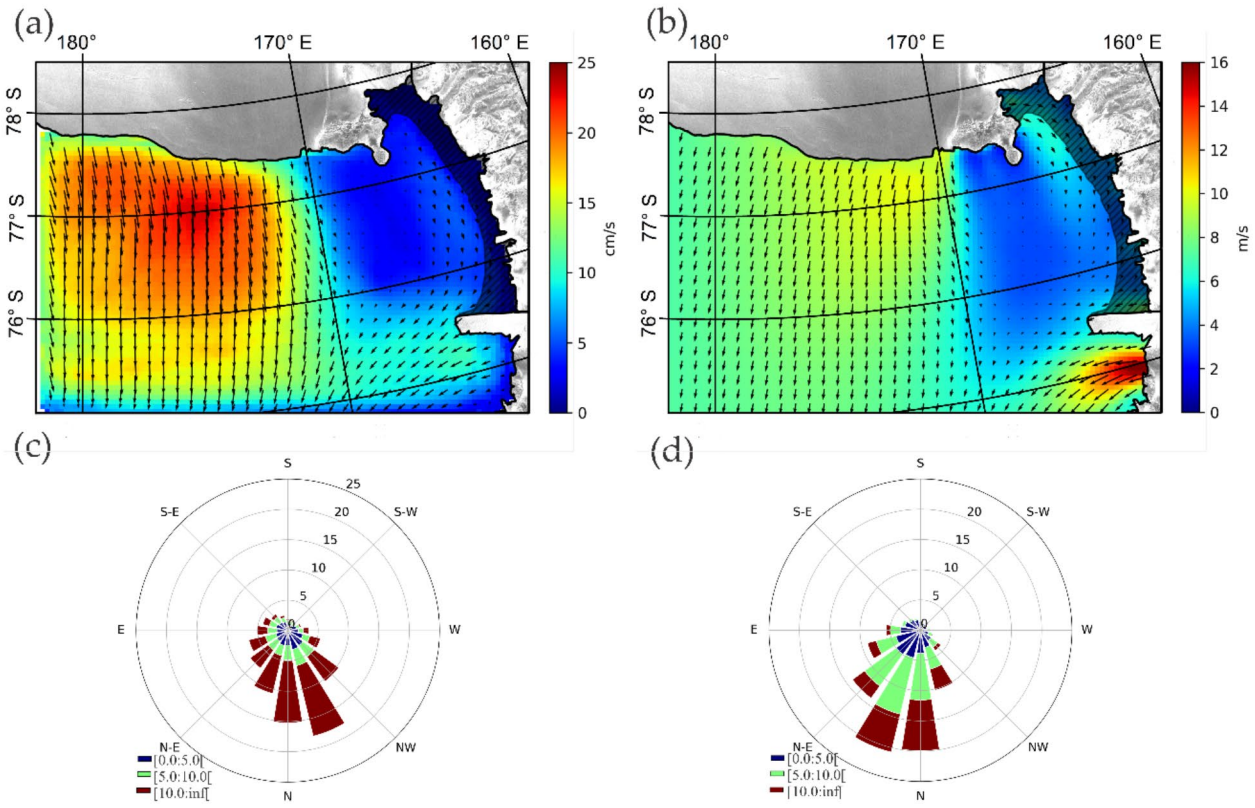

Fig. 4 (a) Mean sea ice velocity calculated from the available satellite-derived vectors (b) Mean wind velocity field from AMPS model output (c) Sea ice motion roses and (d) Wind roses from 2002–2012 (every third vector has been shown)

(~ 10 m/s) and MSP (~ 6 m/s). The overall responses (speed and direction) are displayed as sea ice motion roses and wind roses in Fig. 4c and d, respectively. The directional convention for plotting the roses is identical to the vectors in the polar-stereographic coordinate system. The wind roses show that the mean sea ice velocity is 10–20 degree to the left of the wind speed.

3.3 Spatial correlations between sea ice drift and wind speed

To examine the response of sea ice drift to wind, at every pixel the sea ice speed has been compared with the corresponding wind speed. The Pearson correlation coefficients (R) have been calculated over the entire observational period at each pixel and the spatial distributions are shown in Fig. 5a. This allows us to identify the variance of the sea ice velocities that can be explained by wind velocities. Correlation coefficients were found (R = 0.7) and (R = 0.5) in the RSP and MSP, respectively. Based on Fig. 5a, we can see that the correlation is high in the area of the RSP. However, the correlation is weakest (R = 0.3) in the lee of Ross Island. The low correlation coefficients close to the RIS and in some areas of TNBP are likely due to open water. During the time of opening of the polynya, the sea ice tracking algorithm is unable to find the prominent features for the correlation scheme used. This is further supported by the fact that fewer sea ice drift vectors were obtained in these regions (e.g., TNBP in Fig. 3b). We also note that there were fewer image pairs available that covered the TNBP area (Fig. 2b).

The sensitivity of the sea ice to wind forcing has been evaluated by plotting the gradient (slope) of the least square linear regression fit between sea ice speed and wind speed and is shown in Fig. 5b, which is related to the scaling factor (F). There is a significant contrast of high to low F values from east to west; we interpret this as windier areas having high F values in regions corresponding to thin and less compact sea ice (Steele et al., 1997).

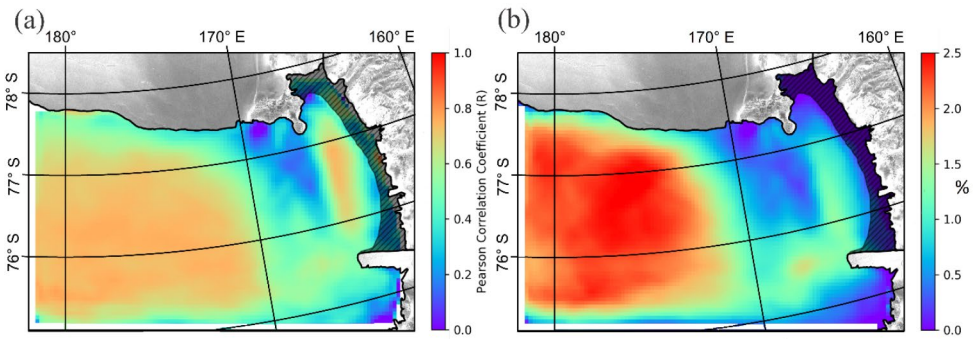

Fig. 5 (a) Correlation map between sea ice drift speed and wind speed from 2002–2012 (b) Sensitivity of the relationship is shown by plotting the gradient of the least square linear fit which is the scaling factor (F). Fast ice is masked by the hatched area as in Fig. 1

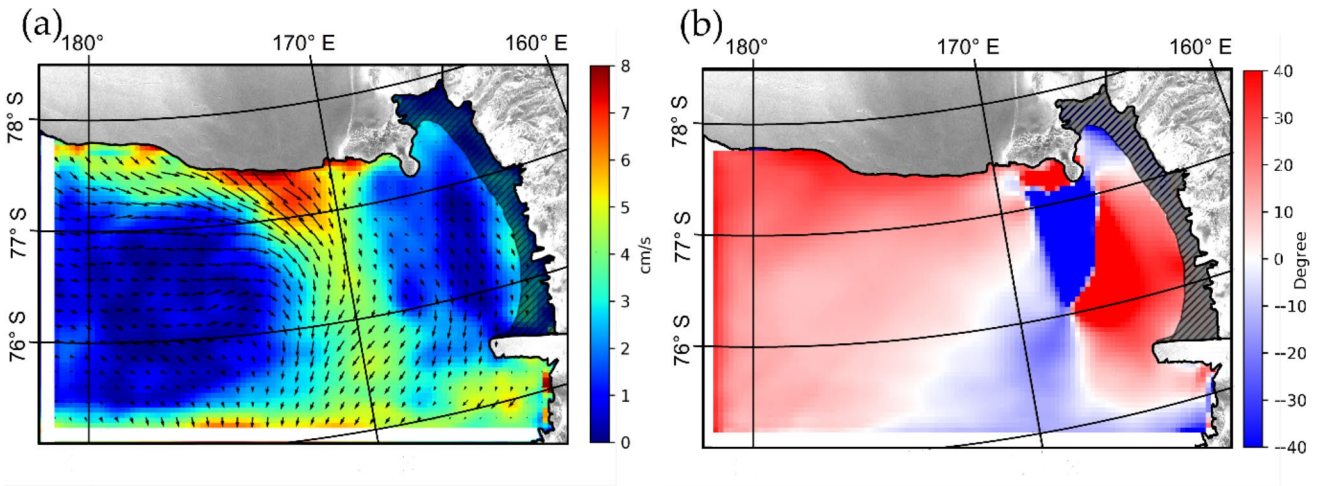

Fig. 6 (a) The residual of the linear relation between wind speed and sea ice speed over the study area from 2002–2012 (every third vector has been shown) (b) Angle deviation (θ) between sea ice drift and wind. Positive angle deviation means that sea ice drift to the left of the wind; otherwise, it is negative

3.4 Residual factor and angle deviation

The constant term of the first-order linear regression between the sea ice speed and wind speed (Fig. 6a) can be connected to the underlying estimated ocean currents by ignoring the internal stresses (Smedsrud et al., 2011) (Eq. 2). However, these values insufficiently describe the ocean currents as they also include other factors explained in Sect. 2.1. We discuss the spatial variability in this residual in Sect. 4. The turning angle (θ) is also calculated by subtracting the wind angle of each vector from the sea ice vector angle and is shown in Fig. 6b. The positive angles show that sea ice drifts to the left of the wind velocity as expected due to the influence of the Coriolis force. Deviations from this rule indicate the influence of other dominant factors resulting in a low directional constancy described in the next section.

3.5 Directional constancy in sea ice and wind field

Variations in the wind fields also potentially play an important role in the sea ice drift. We have therefore further examined the variability in the correlation areas by analyzing the persistence of the vector fields using the directional constancy (DC) (Jolly et al., 2016). DC is defined as the ratio of the vectorial average speed to the mean speed. Zero indicates a high variation in the sea ice drift or wind field, while one shows a persistent field. If u and v are the meridional and zonal components of the velocity vector, then DC is defined as:

$$DC = \frac{\sqrt{\left(\bar{u}^2 + \bar{v}^2\right)}}{\frac{1}{N}\sum_{i=1}^{N}\left(\sqrt{(u_i^2 + v_i^2)}\right)} \tag{3}$$

where, $\bar{u}$ and $\bar{v}$ represent vectorial averages of the zonal and meridional winds, respectively, and N is the total number of observations. The DC of the sea ice drift vectors and wind vectors calculated from 2002 to 2012 using equation-3 are shown in Fig. 7a and b. Examination of the DC patterns in Fig. 7 relative to the correlations in Fig. 5a suggest that the broadest low correlation region of Fig. 4a in the lee of Ross Island can potentially be explained by the variable wind vectors in this region which also directly correlate to low DC values in the sea ice drift field. The correlations between the sea ice drift and wind are highest when the winds are persistent and low when the winds are variable, suggesting that the consistency of wind vectors as measured by directional constancy may be important in identifying the response of sea ice drift to winds.

3.6 Classification of subregions based on sea ice variables

For a simpler interpretation of our results and the underlying physical controls, we sub-divide the study area objectively into regions of similar wind-to-drift relationships. Because wind is a primary driver of pack ice morphology in the area, this will potentially result in regions of similar average sea ice and deformation characteristics. The distributions of mean sea ice velocity, correlation, sensitivity, and directional constancy of sea ice drift in Figs. 4a and 5a and b, and 7a, respectively, form a four-dimensional vector space which are input to an unsupervised k-means classifier (Tou and Gonzalez, 1974) as a proof of concept (Coggins et al., 2014). All input variables were normalized and scaled to 8-bit prior to classification to ensure equal weighting of each variable. A minimum of four and a maximum of eight classes were chosen for the fully automatic classification. The maximum standard deviation of the Euclidian vector distances to the cluster centre in each class was constrained to be less than 10%. The iterative classifier determines an optimal number of six classes by minimizing the class standard deviations within clusters and by maximizing the statistical differences between the clusters. The resulting classes turn out to be very robust and are shown as subregions in Fig. 8a. The standard deviations in each class vary from 3.44% (subregion-1) to 8.83% (subregion-4). Different wind regimes, sea ice conditions, and available free space for sea ice advection seem to differentiate the different sea ice drift regimes. The average classification parameters for each subregion are shown in Table 1 together with the mean

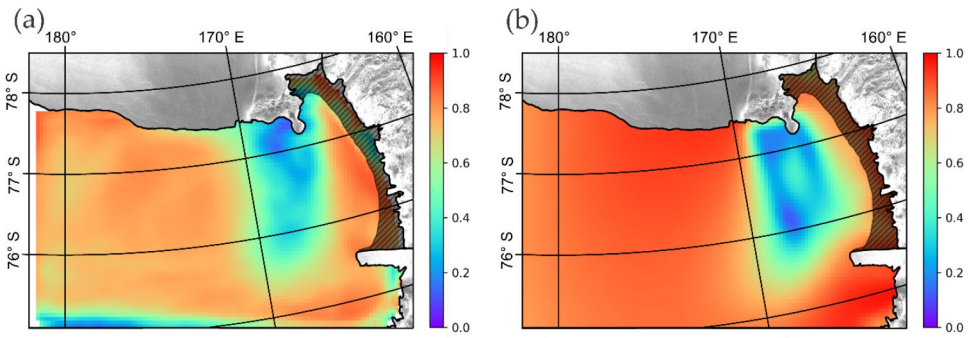

Fig. 7 Directional constancy (DC) calculated for 2002–2012 using equation-3 for (a) the sea ice drift field and (b) wind field

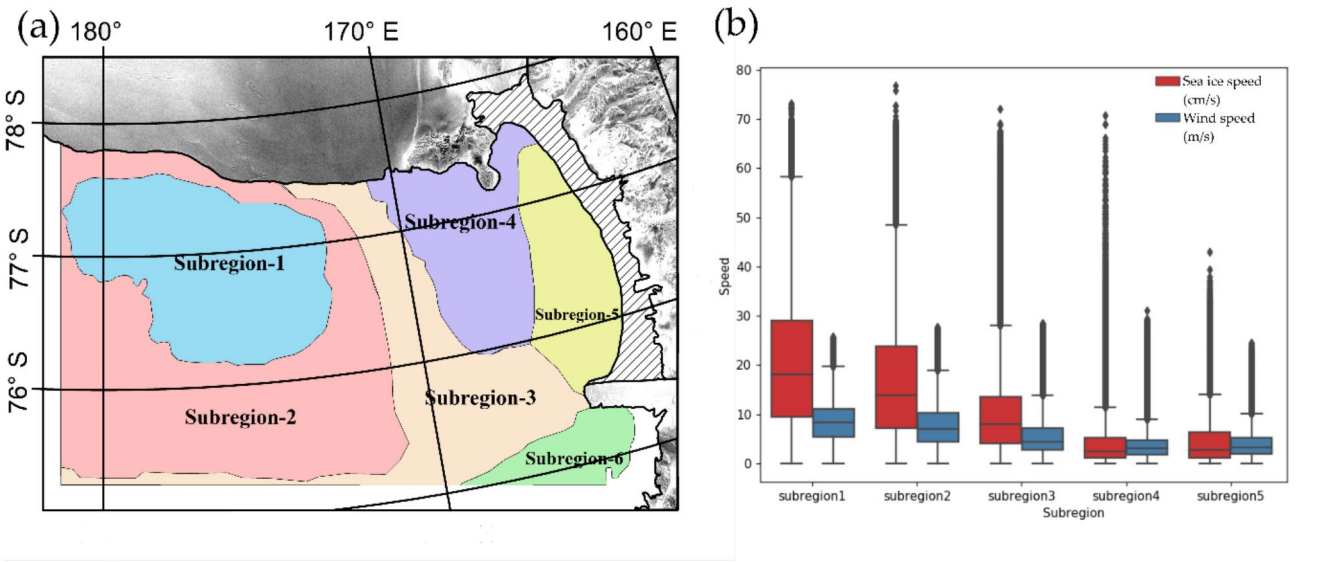

Fig. 8 (a) Distribution of the study area into subregions based on an unsupervised k-means classification (b) Mean sea ice speed (red) in cm/s and mean wind speed (blue) in m/s for the subregions with the bars showing the variability and individual point are showing the speed occasions that occurred rarely. Subregion-6 is not presented here, as it is not represented due to a lack of coverage and unstable features

Table 1 Averages and standard deviations of correlation coefficients (R), scaling factor (F), residual factor, sea ice speed, wind speed, and angle deviations (θ) for five subregions (Fig. 8a) as calculated from Figs. 4a and b, 5a and b and 6a, and 6b respectively

Subregion	Sea ice speed (cm/s)	Wind speed (m/s)	R	F (%)	Residual factor (cm/s)	θ (degrees)
Subregion-1	20.24 ± 1.17	8.68 ± 0.63	0.69 ± 0.06	2.24 ± 0.23	1.52 ± 1.42	16.81 ± 6.54
Subregion-2	16.30 ± 1.63	7.98 ± 0.69	0.70 ± 0.08	1.94 ± 0.35	1.88 ± 1.72	10.11 ± 9.86
Subregion-3	10.21 ± 2.30	6.16 ± 1.76	0.54 ± 0.09	1.10 ± 0.27	3.99 ± 1.22	1.75 ± 15.28
Subregion-4	4.10 ± 1.63	4.28 ± 1.76	0.28 ± 0.12	0.41 ± 0.19	2.54 ± 1.42	-18.93 ± 74.43
Subregion-5	4.68 ± 1.05	4.32 ± 0.73	0.54 ± 0.14	0.86 ± 0.33	1.18 ± 0.90	30.10 ± 20.55
Weighted mean	12.03 ± 6.22	6.99 ± 2.09	0.56 ± 0.21	1.32 ± 0.81	2.44 ± 1.90	3.89 ± 33.48

values of wind speed, correlation coefficients (R), the scaling factor (F), the residual factor, and the angle deviations.

Figure 8b shows box-plots of the mean and the variation in the sea ice speed and wind speed in the different subregions. The maximum possible values for wind speed are similarly high for all subregions (around 30 m/s), whereas the mean values are gradually decreasing from region 1 to 3. Lower but similar mean values are observed in subregions 4 and 5. The possible maximum sea ice drift is similar in subregions 1 to 4 (around 70 cm/s), but the mean values gradually decrease from subregions 1–4. Maximum and mean sea ice drift is lowest in subregion-5. However, subregion-6 is not described because of the high frequency of open water in this region which means sea ice motion vectors were not calculated often.

4 Discussion

We exploited the high temporal and spatial details of sea ice motion in the complex study area of the South-western Ross Sea region. Using four variables, solely derived by sea ice drift and its relation to wind, we are able to distinguish distinct sea ice regions by automatic classification, which visually closely resembles the major sea ice zones found in an earlier study based on radar and thermal satellite imagery (Hollands and Dierking, 2016 and their Fig. 1). This technique has been applied to the western Ross Sea region, in principle it could also be applied to any other region around Antarctica where relevant satellite and AMPS data are available. In this section, we discuss in more detail the relationship between wind and ice drift in the classified subregions, and reflect on possible effects on sea ice morphology. The discussion is concluded with an assessment of the residual between wind and ice drift.

Statistically significant Pearson correlation coefficients (R) were calculated between wind model output data set

and sea ice drift speed of large portions of our study area from April to October, 2002–2012 (Fig. 5a). Another metric that defines the dependency of sea ice drift on wind speed is the scaling factor (F) between sea ice drift speed and wind speed. Nevertheless, to include the directional effects in the analysis we calculated the directional constancy in sea ice drift (DC). We used these three variables and sea ice drift speed (DS) to perform the k-means classification (Fig. 8a), which results in six characteristic data clusters with distinct differences in the mean sea ice properties. We exclude subregion-6 from the discussion, as the strong katabatic wind flow, clearly visible in Fig. 4b, is not evident in the sea ice drift pattern. This is likely a result of the insufficient satellite data coverage in this highly dynamic area and the high occurrence of open water precluding sea ice drift estimates (Fig. 2b).

Subregions 1 and 2 represent relatively free-drifting areas of sea ice dominated by the RIS air stream (Dale et al., 2017) as inferred from the robust relationship between sea ice drift and winds resulting in the highest R values. Sea ice motion in these subregions is clearly determined by the dominant southerly winds from the RIS. F and DS are highest in subregion-1 followed by subregion-2, which indicates thinner and more mobile sea ice in this area similar to the finding by Kwok et al. (2007). F is high in the areas that can be regarded as relatively freely drifting areas (subregion-1 and subregion-2). The spatial variability of F in these subregions is likely due to variations in the sea ice internal stresses that depend on sea ice concentration, thickness, and deformation (Hibler, 1986, Kimura and Wakatsuchi, 2000). In these regions, sea ice moves at around 2% of the rate of the wind speed. Thin ice thermodynamically formed in the RSP starts rafting and experiences leads and cracks, and easily breaks into floes when advected from subregion-1 towards the north, where the ice is thicker. A narrow band between subregion-1 and RIS is associated with subregion-2, which is probably related to the edge of the RISresulting in reduced wind forcing. The same spatial pattern is evident in Figs. 4a and 5a and b, and 6a.

Subregion-3 is the area where the classification shows medium values close to the mean for all classification variables (Table 1). This area was found by Hollands and Dierking (2016) to be a deformation zone between the three polynyas, where ice can grow to large thickness due to a convergent ice regime and low displacement between polynya events (Rack et al., 2020). Ice in this deformation zone responds differently to the wind forcing compared to other zones. Subregion-4 is located in the lee of Ross Island experiencing highly variable winds and therefore has very low directional constancy in ice drift. The drift speed and sensitivity to the wind are lowest in this region. Also, a weak correlation coefficient of ($R = 0.28$) is found in the lee of Ross Island. To further investigate the underlying reasons for the low correlation coefficients in this region, DC maps for sea ice drift and wind velocity were examined. On the used time-scale of one day repeat pass images, both DC maps identify very variable winds and sea ice drift directions in the lee of Ross Island, which could explain the low correlation coefficients in that area. Effectively, the lack of persistent wind forcings in this region has an impact on sea ice drift and deformation in this region. Therefore, subregion-4 can be refereed as a random drift area. Thick sea ice at high concentration probably result in high internal stress and ultimately lower F values in subregion-4 (Fig. 5b). Another interesting aspect is that if we compare these F values with the correlation coefficients (Fig. 5b and a) we found nearly the same spatial variability. This means that high R values are related to high F values likely representing relatively thin ice during periods with polynya activity.

The sea ice in subregion-5 is formed in the McMurdo Sound polynya and drifts parallel to the coast north and northeast. Southerly winds in this area are also responsible for the opening of the MSP. The sea ice starts drifting from the MSP due to relatively persistent winds of that region with the fast ice on its western side. After drifting for 140 km it experiences a lower wind regime, and sea ice converges and accumulates south of the Drygalski ice tongue also meeting with ice from zone 3 creating a deformational ice zone (Hollands and Dierking, 2016). It is ridging into thicker ice as compared to the sea ice formed in the polynya region (Rack et al., 2020). Conversely, subregion-6 appeared as a separate region due to the dominant winds from the TNBP. However, the classification in this area is not well constrained as only a few motion vectors are available in this very dynamic area (Fig. 2b). Our statistical analysis for subregion-6 is therefore inconclusive. However, the sea ice drift in subregion-6 can be explained by the strong katabatic winds, which advect the sea ice towards the east and northeast (Fig. 4b of this study; Hollands and Dierking, 2016).

These spatial correlations derived from high–resolution data sets are slightly higher than reported before (Holland 2012, Kimura 2004) as the real complexity and fine-scale movement of sea ice appears to be captured by high-resolution sea ice drift data sets. The study area includes a coastal region in which sea ice drift is mostly not considered as entirely freely drifting, but the relatively high correlation coefficients show that the sea ice motion is predominantly wind-driven. High correlations also illustrate that a linear sea ice to wind relationship described by Thorndike and Colony (1982) is capable of approximating the sea ice drift observed (Dale et al., 2017). The seasonality has not been detected in the correlation strength, likely due to the limited number of available images. Kimura (2004) also did not report any seasonal effects.

The constant-term of the first-order sea ice speed and wind speed relationship (Fig. 6a) includes the ocean currents and contributions from other factors (such as internal ice stresses, and measurement errors). In the absence of other factors such as internal stresses and mean errors, the constant term of the derived linear relationship between sea ice drift and wind (Fig. 6a) corresponds to ocean currents (Smedsrud et al., 2011). This assumes that drift during periods without wind is driven solely by ocean currents neglecting other forces. To examine the residual factor we analysed the speed, and direction of near surface ocean current model data obtained from the National Institute of Water & Atmospheric Research (NIWA) ocean model (Madec, 2015). The daily ocean current data are provided in a polar-stereographic coordinate system with a nominal spatial resolution of 1/15 degree. We found that the long-term average of the modelled ocean current alone is unable to explain the deficit in the average (2002 to 2012) sea ice drift and wind speed relationship. The regional variability is not only caused by ocean currents, but also includes other factors like sea ice properties and stochastic components (Rampal et al., 2009). However, the spatial variations in the residual varies between subregions. Deformed subregion-3 resulted in high residual values, followed by subregion-4 with lower values. Subregions 1, 2, and 5 showed the minimum residual. By using the satellite and model data, it is challenging to separate the influence of the driving ocean current force from other forces. Although beyond the scope of this study, future analysis should consider inclusion of sea ice internal stresses to answer this question.

5 Conclusions

We have investigated the ice dynamics in one of the most productive areas of sea ice formation in Antarctica where the interaction of three polynyas controls ice deformation. The role of atmospheric forcing in the advection of sea ice from the coastal areas in the Western Ross Sea has been studied by analysing satellite-derived high-resolution sea ice drift and wind model output data sets from April to October, 2002–2012. The question of dependency of sea ice drift on the wind is of fundamental importance; it tells us about the sensitivity of sea ice drift on the various forces applied. For the detailed and synoptic comparison of sea ice dynamics, we explored the spatial variations of the correlation coefficients and evaluated the sensitivity of sea ice motion to the prevailing winds and ocean currents by plotting the relational parameters (scaling factor, angle deviation, and sensitivity of the correlation coefficients). To achieve this, we utilized ten years of unique high-resolution Envisat SAR satellite data and AMPS surface winds. We therefore conclude that the sea ice morphology in this area is highly dependent on wind-driven sea ice dynamics. The small residual between wind and ice drift illustrates that the ocean currents likely play only a minor role for sea ice drift in this area.

The classified subregions depend on both the drift speed and the directional constancy of drift. Both variables are highly correlated with the wind, which is controlled by the topography of the region and the presence and position of low pressure systems (Coggins et al., 2014; McDonald and Cairns, 2020). The geographic position of the Ross Ice Shelf air stream is concurrent with the high correlation coefficients just north of the Ross Ice Shelf, whereas variable winds north of Ross Island and near the Victoria Land coastline weaken the drift-wind relationship. Wind forcing on the sea ice can largely be explained by a linear relationship for the steady-state and nearly freely drifting sea ice. Our study is solely based on products of ice drift and wind, which possibly identify coherent regions of ice thickness distribution as a consequence of deformational growth. Independent information on sea ice thickness is required to support this hypothesis and will be the focus of future efforts. This study emphasizes the need for making use of high spatial resolution satellite data to improve our understanding of sea ice deformation in complex coastal areas. Nevertheless, our method did not allow to find a strong correlation between wind and sea ice drift in the Terra Nova Bay region. Satellite revisit times even shorter than 24 h would probably increase the correlation between wind and sea ice drift in this highly dynamic area, and would possibly allow us to better constrain the drift to wind relationship as an input for the proposed sea ice classification and parameterization.

Acknowledgements The Envisat satellite data are received within the ESA research project 30877 titled “Sea ice dynamics in the area of the Ross Sea Polynya” (PI W. Rack). Antarctic Mesoscale Prediction System (AMPS) wind velocity data set are freely available and downloaded from http://polarmet.osu.edu/AMPS/. The authors thank Erik Behrens (National Institute of Water & Atmospheric Research - NIWA) for model outputs of surface ocean currents and fruitful discussions.

Funding The research is supported by the University of Canterbury doctoral scholarship, the Deep South National Science Challenge, New Zealand, and the Antarctic Science Platform.

Open Access funding enabled and organized by CAUL and its Member Institutions

Declarations

Conflict of interest The authors declare no conflict of interest.

References

Aulicino, G., Wadhams, P., and Parmiggiani, F.: SAR pancake ice thickness retrieval in the terra nova bay (Antarctica) during the PIPERS Expedition in winter 2017, Remote Sensing, 11, 2510, 2019.

Blanchard-Wrigglesworth, E., Roach, L. A., Donohoe, A., and Ding, Q.: Impact of winds and Southern Ocean SSTs on Antarctic sea ice trends and variability, Journal of Climate, 34, 949–965, 2021.

Bromwich, D. H., Monaghan, A. J., Manning, K. W., and Powers, J. G.: Real-time forecasting for the Antarctic: An evaluation of the Antarctic Mesoscale Prediction System (AMPS), Monthly Weather Review, 133, 579–603, 2005.

Coggins, J. H., McDonald, A. J., and Jolly, B.: Synoptic climatology of the Ross Ice Shelf and Ross Sea region of Antarctica: k-means clustering and validation, International journal of climatology, 34, 2330–2348, 2014.

Dale, E. R., McDonald, A. J., Coggins, J. H., and Rack, W.: Atmospheric forcing of sea ice anomalies in the Ross Sea polynya region, The Cryosphere, 11, 267–280, 2017.

Doble, M. J., and Wadhams, P.: Dynamical contrasts between pancake and pack ice, investigated with a drifting buoy array, Journal of Geophysical Research: Oceans, 111, 2006.

Farooq, U., Rack, W., McDonald, A., and Howell, S.: Long-Term Analysis of Sea Ice Drift in the Western Ross Sea, Antarctica, at High and Low Spatial Resolution, Remote Sensing, 12, 1402, 2020.

Heil, P., and Allison, I.: The pattern and variability of Antarctic sea-ice drift in the Indian Ocean and western Pacific sectors, Journal of Geophysical Research: Oceans, 104, 15789–15802, 1999.

Hibler, W.: Ice dynamics, in: The geophysics of sea ice, Springer, 577–640, 1986.

Holland, P. R., and Kwok, R.: Wind-driven trends in Antarctic sea-ice drift, Nature Geoscience, 5, 872–875, 2012.

Hollands, T., and Dierking, W.: Dynamics of the Terra Nova Bay Polynya: The potential of multi-sensor satellite observations, Remote Sensing of Environment, 187, 30–48, 2016.

Holmes, C. R., Holland, P. R., and Bracegirdle, T. J.: Compensating biases and a noteworthy success in the CMIP5 representation of Antarctic sea ice processes, Geophysical Research Letters, 46, 4299–4307, 2019.

Howell, S.E., Brady, M., and Komarov, A.K.: Generating large-scale sea ice motion from Sentinel-1 and the RADARSAT Constellation Mission using the Environment and Climate Change Canada automated sea ice tracking system, The Cryosphere, 16, 1125-1139, 2022.

Jacobs, S. S.: Bottom water production and its links with the thermohaline circulation, Antarctic Science, 16, 427, 2004.

Jolly, B., Mcdonald, A. J., Coggins, J. H., Zawar-Reza, P., Cassano, J., Lazzara, M., Graham, G., Plank, G., Petterson, O., and Dale, E.: A validation of the Antarctic mesoscale prediction system using self-organizing maps and high-density observations from SNOWWEB, Monthly Weather Review, 144, 3181–3200, 2016.

Kimura, N., and Wakatsuchi, M.: Relationship between sea-ice motion and geostrophic wind in the northern hemisphere, Geophysical Research Letters, 27, 3735–3738, 2000.

Kimura, N.: Sea ice motion in response to surface wind and ocean current in the Southern Ocean, Journal of the Meteorological Society of Japan. Ser. II, 82, 1223–1231, 2004.

Komarov, A. S., and Barber, D. G.: Sea ice motion tracking from sequential dual-polarization RADARSAT-2 images, IEEE Transactions on Geoscience and Remote Sensing, 52, 121–136, 2014.

Kwok, R.: Ross Sea ice motion, area flux, and deformation, Journal of climate, 18, 3759–3776, 2005.

Kwok, R., Comiso, J. C., Martin, S., and Drucker, R.: Ross Sea polynyas: Response of ice concentration retrievals to large areas of thin ice, Journal of Geophysical Research: Oceans, 112, 2007.

Kwok, R., Pang, S. S., and Kacimi, S.: Sea ice drift in the Southern Ocean: Regional patterns, variability, and trends, Elem Sci Anth, 5, 2017.

Leppäranta, M.: The drift of sea ice, Springer Science & Business Media, 2011.

Madec, G.: NEMO ocean engine, 2015.

McDonald, A. J., and Cairns, L. H.: A New Method to Evaluate Reanalyses Using Synoptic Patterns: An Example Application in the Ross Sea/Ross Ice Shelf Region, Earth and Space Science, 7, e2019EA000794, 2020.

Notz, D.: Challenges in simulating sea ice in Earth System Models, Wiley Interdisciplinary Reviews: Climate Change, 3, 509–526, 2012.

Parish, T. R., Cassano, J. J., and Seefeldt, M. W.: Characteristics of the Ross Ice Shelf air stream as depicted in Antarctic Mesoscale Prediction System simulations, Journal of Geophysical Research: Atmospheres, 111, 2006.

Parkinson, C. L.: A 40-y record reveals gradual Antarctic sea ice increases followed by decreases at rates far exceeding the rates seen in the Arctic, Proceedings of the National Academy of Sciences, 116, 14414–14423, 2019.

Powers, J. G., Manning, K. W., Bromwich, D. H., Cassano, J. J., and Cayette, A. M.: A decade of Antarctic science support through AMPS, Bulletin of the American Meteorological Society, 93, 1699–1712, 2012.

Rack, W., Price, D., Haas, C., Langhorne, P. J., and Leonard, G. H.: Sea Ice Thickness in the Western Ross Sea, Geophysical Research Letters, e2020GL090866, 2020.

Rampal, P., Weiss, J., and Marsan, D.: Positive trend in the mean speed and deformation rate of Arctic sea ice, 1979–2007, Journal of Geophysical Research: Oceans, 114, 2009.

Roach, L. A., Dörr, J., Holmes, C. R., Massonnet, F., Blockley, E. W., Notz, D., Rackow, T., Raphael, M. N., O'Farrell, S. P., and Bailey, D. A.: Antarctic sea ice area in CMIP6, Geophysical Research Letters, 47, e2019GL086729, 2020.

Smedsrud, L. H., Sirevaag, A., Kloster, K., Sorteberg, A., and Sandven, S.: Recent wind driven high sea ice area export in the Fram Strait contributes to Arctic sea ice decline, The Cryosphere, 5, 821–829, 2011.

Steele, M., Zhang, J., Rothrock, D., and Stern, H.: The force balance of sea ice in a numerical model of the Arctic Ocean, Journal of Geophysical Research: Oceans, 102, 21061–21079, 1997.

Thomas, D.: The quality of sea ice velocity estimates, Journal of Geophysical Research: Oceans, 104, 13627–13652, 1999.

Thorndike, A., and Colony, R.: Sea ice motion in response to geostrophic winds, Journal of Geophysical Research: Oceans, 87, 5845–5852, 1982.

Tou, J., and Gonzalez, R.: Pattern Recognition Principles, Addison-WesleyPubl, Comp., Massachusetts, 1974.

Turner, J., Phillips, T., Marshall, G. J., Hosking, J. S., Pope, J. O., Bracegirdle, T. J., and Deb, P.: Unprecedented springtime retreat

of Antarctic sea ice in 2016, Geophysical Research Letters, 44, 6868–6875, 2017.
Van Woert, M. L.: Wintertime dynamics of the Terra Nova Bay polynya, Journal of Geophysical Research: Oceans, 104, 7753–7769, 1999.
Weiss, J.: Drift, deformation, and fracture of sea ice: a perspective across scales, Springer, 2013.